*J. Fluid Mech.* (2002), *vol.* 455, *pp.* 103–127.  
DOI: 10.1017/S002211200100725X Printed in the United Kingdom

# Particle pressures generated around bubbles in gas-fluidized beds

By KHURRAM RAHMAN AND CHARLES S. CAMPBELL

Department of Mechanical Engineering, University of Southern California, Los Angeles, CA 90089-1453, USA

(Received 15 July 1999 and in revised form 10 August 2001)

The particle pressure is the surface force in a particle/fluid mixture that is exerted solely by the particle phase. This paper presents measurements of the particle pressure on the faces of a two-dimensional gas-fluidized bed and gives insight into the mechanisms by which bubbles generate particle pressure. The particle pressure is measured by a specially designed 'particle pressure transducer'. The results show that, around single bubbles, the most significant particle pressures are generated below and to the sides of the bubble and that these particle pressures steadily increase and reach a maximum value at bubble eruption. The dominant mechanism appears to be defluidization of material in the particle phase that results from the bubble attracting fluidizing gas away from the surrounding material; the surrounding material is no longer supported by the gas flow and can only be supported across interparticle contacts which results in the observed particle pressures. The contribution of particle motion to particle pressure generation is insignificant.

The magnitude of the particle pressure below a single bubble in a gas-fluidized bed depends on the bubble size and the density of the solid particles, as might be expected as the amount of gas attracted by the bubble should increase with bubble size and because the weight of defluidized material depends on the density of the solid material. A simple scaling of these quantities is suggested that is otherwise independent of the bed material.

In freely bubbling gas-fluidized beds the particle pressures generated behave differently. Overall they are smaller in magnitude and reach their maximum value soon after the bubble passes instead of at eruption. In this situation, it appears that the bubbles interact with one another in such a way that the defluidization effect below a leading bubble is largely counteracted by refluidizing gas exiting the roof of trailing bubbles.

## 1. Introduction

The particle pressure may be thought of as the force per unit area exerted by the particle phase of a multiphase mixture and, as such, reflects the total momentum transport that can be attributed to the motion of particles and their interactions. It has a direct analogy in the kinetic theory of gases in which the pressure acting on a surface is visualized as a result of the impact of molecules. The same picture can be applied to particle–fluid situations with the particles taking the place of molecules. The only difference between the two cases is that solid particles, in addition to short duration collisional impacts, transmit a force via long duration contacts. For example, the weight of a particle, or an assembly of particles resting on a surface is

also a particle pressure. In this context, macroscopic solid particles are fundamentally different from molecules in that solid particles can exert short-range elastic forces across contact points with other solid particles or with bounding surfaces.

The particle pressure is an important quantity in multiphase flow modelling which generally treats the separate phases as interpenetrating continua. This technique involves writing separate conservation equations for each phase. Typically the equations for the fluid and solid phases look individually like the usual single-phase equations with the addition of a coupling term, $F$, that accounts for interphasial forces:

$$\rho_f \left( \frac{\partial \boldsymbol{V}_f}{\partial t} + \boldsymbol{V}_f \cdot \nabla \boldsymbol{V}_f \right) = \nabla \cdot \boldsymbol{\tau}_f + \rho_f \epsilon \boldsymbol{g} + \boldsymbol{F}, \tag{1.1}$$

$$\rho_p (1-\epsilon) \left( \frac{\partial \boldsymbol{V}_p}{\partial t} + \boldsymbol{V}_p \cdot \nabla \boldsymbol{V}_p \right) = \nabla \cdot \boldsymbol{\tau}_p + \rho_p (1-\epsilon) \boldsymbol{g} - \boldsymbol{F}. \tag{1.2}$$

Here $\epsilon$ is the void fraction (the volume fraction of the fluid phase), $\boldsymbol{V}_f$ and $\boldsymbol{V}_p$ are the fluid and particle velocities, $\rho_f$ and $\rho_p$ are the fluid and particle densities, and $\boldsymbol{\tau}_f$ and $\boldsymbol{\tau}_p$ are the fluid- and particle-phase stress tensors. This work is concerned with $\boldsymbol{\tau}_p$, which strictly should be interpreted as the stress tensor induced by the particle phase that also acts on the particle phase. One of the difficulties in accurately applying equations (1.1) and (1.2) is that there is very little understanding of how to model particle-phase stresses. This study presents experimental measurements of the component of the particle stresses that is exerted normal to the walls of a fluidized bed.

The behaviour of the particle pressure can have significant effects on the behaviour of multiphase systems. Early studies (Jackson 1963; Pigford & Baron 1965; Murray 1965) on the stability of a fluidized bed ignored the effects of interparticle forces and declared the fluidized state to be intrinsically unstable regardless of the fluid–particle system involved. Further research (Anderson & Jackson 1968; Garg & Pritchett 1975; Jackson 1985; Foscolo & Gibilaro 1987; Batchelor 1988; Ham *et al.* 1990; Rietema & Piepers 1990; Rietema, Cottaar & Piepers 1993; Koch & Sangani 1999) has led to the speculation that the particle pressure is responsible for the stability of fluidized beds, reflecting the possibility that instabilities may grow or be damped through the forces transmitted within the particle phase itself. Anderson & Jackson (1968), Garg & Pritchett (1975), Foscolo & Gibilaro (1987) and Batchelor (1988) have all shown that the 'elasticity' of the particle phase can stabilize the bed. Here, elasticity is defined as $E_p = -(\mathrm{d}P_p/\mathrm{d}\epsilon)$, where $\epsilon$ is the void fraction and $P_p$ is the particle pressure. The larger the magnitude of $E_p$, the larger is the resistance to voidage changes, resulting in a smaller growth rate of voidage waves and this can lead to stable fluidization.

Anderson & Jackson (1968) also showed that the rate of growth of instabilities is strongly affected by the density ratio of the two phases. Consequently, the growth rate is much larger when particles are fluidized by air compared to water, suggesting why almost all gas-fluidized beds are observed to bubble, while bubbling behaviour in liquid-fluidized beds is rare. Agbim, Nienow & Rowe (1971) used magnetized particles, to increase interparticle forces, in a gas-fluidized bed and observed that bubbling was suppressed and the bed showed a regime of stable fluidization. Mutsers & Rietema (1977) proposed that there are interparticle cohesive forces generated by Van Der Walls forces that are certainly significant between small particles and which lead to stable fluidization; this was backed up by experiments on a tilting fluidized bed that exhibited a yielding behaviour even when fluidized. Tsinotides & Jackson (1993) studied cracking catalyst fluidized by gases and, at least for the particles

they studied, the particle assemblies exhibited yield stresses throughout the range of stable behaviour; they concluded that particle contact forces were responsible for stabilization.

But beyond its importance to the science of fluidization and multiphase flows, the particle pressure, as a reflection of the interparticle forces, is also directly relevant to the attrition of particles. Since numerous industrial operations utilize fluidization (e.g. the fluid cracking catalyst (FCC) process), particle attrition is a consideration of much importance, especially if the solid particles are expensive. The dust so produced can also be an environmental hazard requiring the installation of expensive precipitators and filters. Also, solid break-up can clog industrial equipment (e.g. filters, pipes) and diminish the purity of a product by contamination. Another concern is the abrasion of the bed walls and the vessels and pipes inside the bed due to particle contact which might limit equipment life. Again, this abrasion is directly dependent on the particle-phase forces.

There have been few direct measurements of particle pressure in fluidized beds. Rathbone, Ghadiri & Clift (1989) measured transient normal and shear stresses on the surface of a tube in a freely bubbling two-dimensional gas-fluidized bed using a piezo-electric force transducer. The measurements were synchronized with video recordings of bubbles as they rose in the bed. The measurements showed that the largest stress imposed on the tube was when 'packets' of particles, that were transported in the bubble wakes, impinged on the tube surface. Near the bubble nose the stress measured on the tube was comparatively much smaller, and the background stress was even smaller. Thus, a schematic of the stress transient shows a peak corresponding to the arrival of bubble wake particles, followed by a decaying of the stress to a small value. This indicates that the dominant effect causing particle pressure is the direct agitation of particles by bubbles.

Further evidence confirming the effect of bubbles on particle pressure was demonstrated by Campbell & Wang (1991). They measured the average particle pressure exerted on the sidewall of a three-dimensional ($12.7 \times 12.7$ cm ($5 \times 5$ in.) cross-section) gas-fluidized bed. In the packed state the particle pressure decreases as the gas velocity is increased, until it reaches a minimum value at the minimum fluidization velocity. Further increase in the gas velocity, corresponding to the appearance of bubbles, causes the particle pressure to increase until it finally reaches a fixed value and ceases to change with a further increase in gas velocity. This plateau in particle pressure corresponds to the onset of 'slugging', i.e. the bubbles span the full dimensions of the channel and are unable to grow laterally. The results showed a scaling of the particle pressure with the particle density and bubble size for various particle diameters, particle densities, and positions in the bed.

Kumar, Hart & Brennen (1990) and Zenit, Hunt & Brennen (1997) have measured particle pressures in liquid-fluidized beds. Both used high-frequency-response dynamic pressure transducers that measure the individual collisions of particles with the walls. They documented the time-averaged particle pressures for different particle sizes and densities at various concentrations. The results showed that increasing the fluid velocity beyond minimum fluidization causes the particle pressure first to rise, eventually reaching a maximum before falling off. This reflects two competing processes internal to the material. Increasing the fluidizing velocity increases the agitation rate of the particles and consequently increases the strength of the collisions. However, at the same time, it also decreases the density within the bed, and with it the number of particle collisions. Eventually, the number of collisions is reduced to the point that the pressure falls despite the increased strength of each collision. Zenit

*et al.* (1997) also showed that the measured particle pressure scales with the particle dynamic pressure (based on the particle density and terminal velocity). The magnitude of the particle pressure is much smaller in these measurements than in the results of Campbell & Wang (1991). This points out a fundamental difference between liquid (non-bubbling) and gas (bubbling) fluidized beds; that is, the large-scale disturbances generated by bubbles in gas-fluidized beds result in larger particle pressures than the smaller-scale disturbances observed in liquid-fluidized beds.

## 2. The particle pressure transducer

The difficulty in measuring particle pressure in a particle/fluid system is that the total pressure exerted on a surface – the pressure that would be measured with a standard flush-mounted pressure transducer – is the sum of the particle pressure and the pressure exerted by the fluid that resides in the interstices between the particles. Furthermore, in many cases (e.g. fluidized beds or slurry flows) in which the motion is driven by fluid pressure, the particle pressure may be a small fraction of the total. Conceptually, measuring particle pressures is not complicated, nor is the measurement very difficult. Essentially all one has to do is measure the total force acting on a surface and then let that fraction due to the fluid pressure balance itself out. One could make such a measurement by inserting a flush-mounted pressure transducer into the surface (which would sense the total pressure exerted by the particles and the fluid), and then taking the difference between that and a separate pressure transducer that sensed only the pressure of gas admitted through a small port through which particles cannot pass; however, the particle pressure is often such a small fraction of the total (as small as 1%) that the signal would be lost in the noise of the measurement. Thus it is necessary to make the subtraction between the two pressures directly at the point of measurement. Campbell & Wang (1990) described a very simple transducer for this purpose. That probe consisted of a solid diaphragm flush mounted into the wall. Small holes on either side of the diaphragm admitted fluid, but no particles, into a chamber behind the diaphragm. The face of the diaphragm experiences the total pressure exerted by both particles and the fluid, while the rear experiences only fluid forces. Thus, the net deflection of the diaphragm reflects the contribution of the particle forces only. Campbell & Wang (1991) used this probe to carry out time-averaged particle pressure measurements on the vertical sidewalls of a three-dimensional gas-fluidized bed.

Campbell & Wang (1990) showed that there was room for improvement in the dynamic response of their probe to fast changes in the local fluid and/or particle pressures that was attributed to the fluidic resistance from the relatively small area of holes that admitted the gas to the rear of the diaphragm and the large fluidic capacitance of the volume behind the diaphragm. The probe used in this current study is based on the same principle as the Campbell & Wang probe, but virtually eliminates this problem by reducing both the resistance and capacitance of the system. A schematic of this transducer is shown in figure 1. Here, the solid diaphragm of the probe used by Campbell & Wang (1990) is replaced by a screen whose displacement is measured by a transducer. As the screen has orders of magnitude more area than the small holes that surrounded the diaphragm in Campbell & Wang's (1990) design, the resistance to fluid motion through the screen is dramatically reduced. At the same time, the fluidic capacitance of the probe is minimized by making the cavity behind the diaphragm as small as possible. (There is really no need for the cavity to be much thicker than the full range displacement of the diaphragm. Since the maximum

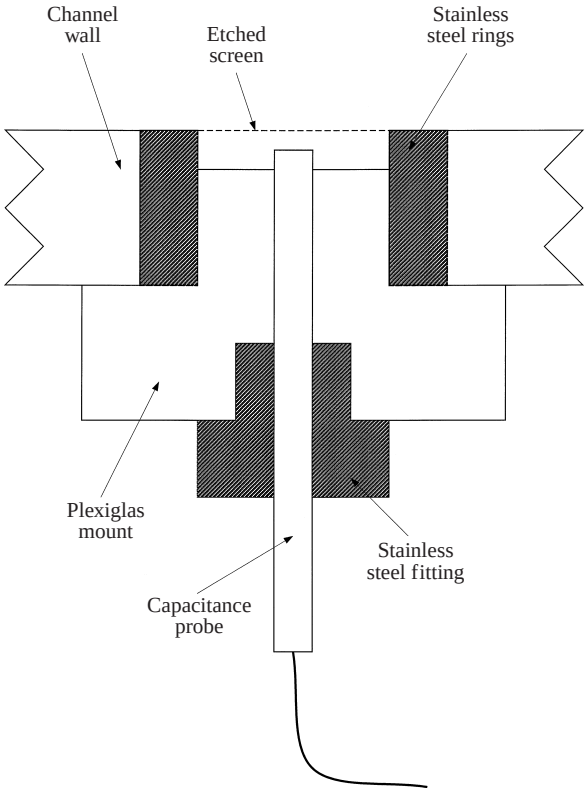


FIGURE 1. A schematic of the particle pressure transducer.

measurable diaphragm motion is determined by the range of the capacitance probe (0.13 mm), the cavity is cut to the same depth.) The tests in Campbell & Rahman (1992) demonstrated that this system did not respond to a fluctuating gas pressure up to frequencies of several kilohertz, while the probe of Campbell & Wang (1990) showed a strong response to the same kinds of signals.

The construction of the probe should be apparent from figure 1. The screen that forms the diaphragm is tensioned and attached to a stainless steel ring by spotwelding. Several versions of the probe have been built with various diaphragm diameters. The probes used for this work used a diaphragm with an effective diameter of 2.54 cm (1.0 in.). The displacement of the diaphragm is measured by an MTI Accumeasure probe with a 0 to 0.13 mm range that determines the displacement of the diaphragm by sensing the capacitance across the air gap between the probe and the diaphragm. Of course, the displacement could also be measured by mounting strain gauges or any other means, but the capacitance measurement was an easy scheme to implement. The 'screen' that serves as a diaphragm is manufactured by Buckbee Mears and was made from a solid aluminium sheet by etching a regular pattern of 70 μm holes. (A more detailed description of the particle pressure transducer can be found in Campbell & Rahman 1992.)

It should be noted that this probe measures the particle forces exerted normal to the vertical wall of the bed. This may well not be the isotropic pressure generated within the bed and may contain deviatoric components. In other words, they represent only one component of the particle stress, $\boldsymbol{\tau}_p$, in equation (1.2).

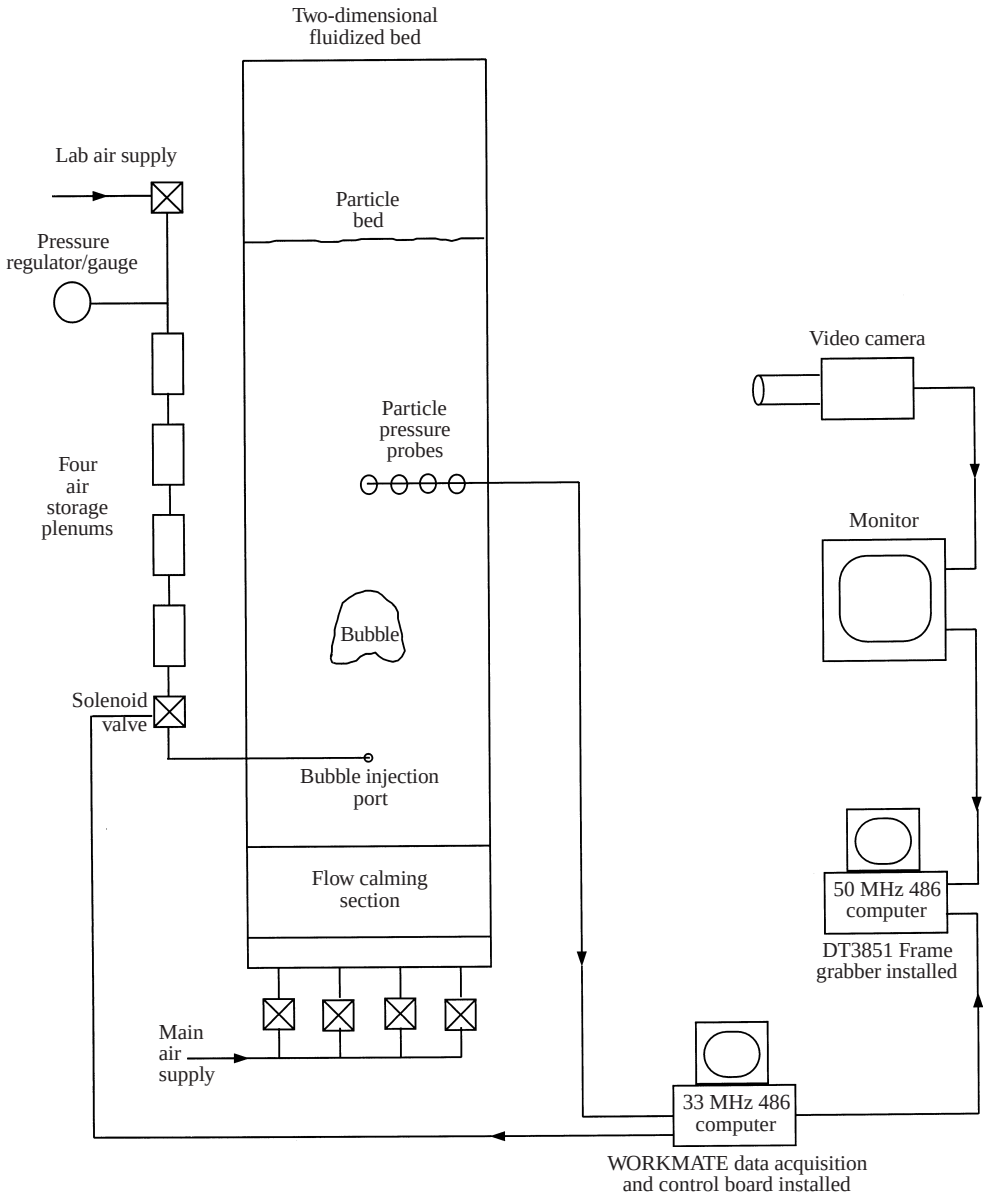


FIGURE 2. A schematic of the two-dimensional fluidized bed, showing the data acquisition and control set-up to inject a bubble, track a bubble and log particle pressure data.

## 3. Experimental set-up

Figure 2 is a schematic of the two-dimensional bed used for the majority of these experiments. The test section is 152 cm (60 in.) high, 46 cm (18 in.) wide, but only 2.5 cm (1 in.) deep. It is fed by an air supply system that passes air through a 10 in. packed bed and several of the Buckbee Mears (2-2-8) 70 μm etched screens are sandwiched between sheets of filter paper to ensure a large pressure drop and a uniform airflow. The airflow is usually set so that the bed is at minimum fluidization conditions. Then bubbles are injected through a screen-covered port, located 23 cm (9 in.) above the

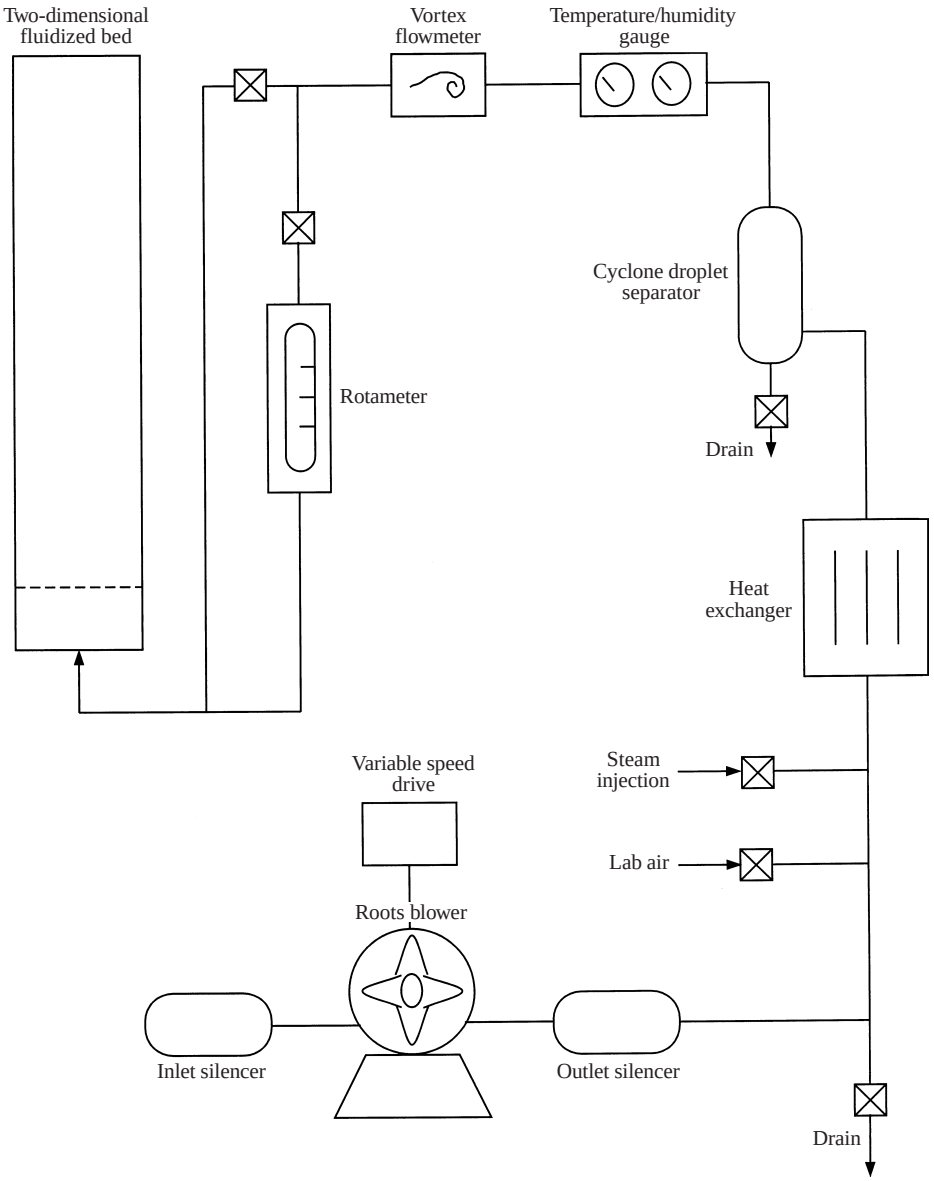


FIGURE 3. The fluidizing air supply set-up.

distributor. The bubble injector consists of a series of plenums which are pressurized through a precision pressure regulator. Firing a solenoid valve admits pressured air into the bed, causing a bubble to form. Different plenum pressures and injection times will discharge different quantities of gas, allowing control over the bubble size. Finally, 25 ports are cut into the face of the channel to admit the particle pressure transducers. Sixteen of the ports are configured in four lines of four, spaced at 15.2 cm (6 in.) intervals above the injection port; in each line, the ports are spaced 5 cm (2 in.) apart, spanning the area from the centre of the bed to one wall. The other nine ports are located at intermediate locations across the bed, in case a finer spatial resolution is required. Four particle pressure probes are available to be inserted in any of the ports.

The fluidizing air (see figure 3) is provided by an M&D Pneumatics 3204 three-lobe Roots-type blower driven by a 5HP variable speed motor so that the flow rate may be controlled by varying the speed of the blower. Steam from a modified pressure cooker can be added to humidify the air so as to eliminate static build-up in the material inside the bed. The flow then travels through a heat exchanger to remove the heat of compression and a small cyclone type device that removes any droplets that may become entrained in the airstream from the steam injection. Then the air passes through a temperature and humidity measuring gauge and, finally, through a Dwyer rotameter, that determines the flow rate.

Bubbles are tracked and followed by an image processing system. The data acquisition and control set-up for the experiment can be seen in figure 2. The image originates in an Image Technology Methods, Datavision 262, video camera. This, in turn, is sampled by a Data Translation 3851 frame grabber. The DT3851 board possesses an external trigger which allows the acquisition of the images to be synchronized with the acquisition of the particle pressure data. The particle pressure data acquisition is performed in a separate computer; digital outputs from the computer are used to trip a relay which injects the bubble and to fire the external trigger of the DT3851, as well as to sample the particle pressure information. This tightly synchronizes the entire experimental process.

Both the acquisition and interpretation of the images are controlled by Data Translation's Global Lab Image Software package. This package provides many powerful image processing options. The most useful for this experiment is the ability to detect and analyse 'particles' (which in this context refers to bubbles). In particular, it locates the centre-of-area of the bubble which is used as a reference for the bubble location, calculates the area of the bubble, the average radius from the centre-of-area, and so on.

## 4. Particle pressure measurements and discussion

Figure 4 shows a time history of the particle pressures measured by the four probes which are located 46 cm (18 in.) above the injection point and 0, 5, 10 and 15 cm along the horizontal direction from the bed centreline (the corresponding plots are shown in order starting at the top of the figure). The test material in this case is 0.5 mm glass beads and the bed height is 109 cm (43 in.) which places 41 cm (16 in.) of material above the probes. The figure is also labelled with the locations where the bubble crosses the probes, as well as the location where the bubble erupts from the surface of the bed. At the time it crosses the probes, the bubble has an equivalent radius of about 9 cm (see figure 5) and thus, the bulk of the bubble crosses the positions of the two innermost probes.

The bed is held at minimum fluidization conditions and the bubble is injected at time = 0 s (on the time axis shown in figure 4) for a duration of 0.2 s. Before the bubble is injected the particle pressure, as measured by all four probes, is approximately constant and has a negligibly small value (always less than 5 mm $H_2O$). The particle pressure along the bed centreline (figure 4*a*) is small above the bubble (time = 0 to about 0.75 s); there is a short-duration initial peak which corresponds to the sudden injection of gas, followed by a period (up to about time = 0.4 s) where the particle pressure value is roughly the same as in an undisturbed bed held at minimum fluidization conditions. But just upstream of the bubble (from time = 0.4 to 0.75 s) there is a small, though noticeable, particle pressure hump. Naturally the particle pressure goes to zero as the bubble crosses the centreline probe (time = 0.75 to 1.2 s,

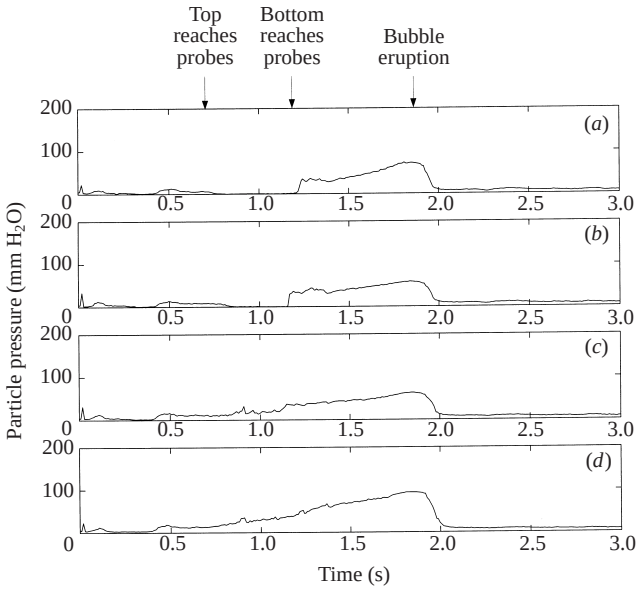


FIGURE 4. The time histories of the particle pressures in a bed of 0.5 mm glass beads. The four plots represent the four probes mounted 46 cm (18 in.) above the injection point and 0, 5, 10, 15 cm from the bed centreline (*a*)–(*d*). The bed height is 109 cm (43 in.) and the effective bubble diameter just before eruption is 25.0 cm (9.8 in.).

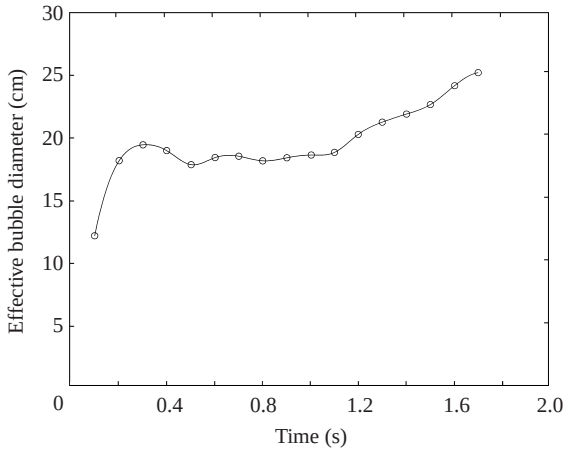


FIGURE 5. The effective bubble diameter as a function of time for the particle pressure measurements shown in figure 4.

figure 4(*a*) as there are no particles present. However the most significant particle pressures are measured below the bubble (from time = 0.75 s until bubble eruption at time = 1.8 s). Note that there is an abrupt increase in particle pressure as the centreline probe encounters the bubble wake, and as the bubble continues its ascent, the particle pressure steadily rises and reaches its maximum value as the bubble erupts from the bed. Figure 4(*b*), which shows the particle pressure measured 5 cm from the bed centreline, is almost identical to figure 4(*a*). But, figures 4(*c*) and 4(*d*) which represent the particle pressure measured by the probes mounted 10 cm and 15 cm from the bed centreline respectively, show a somewhat different picture since

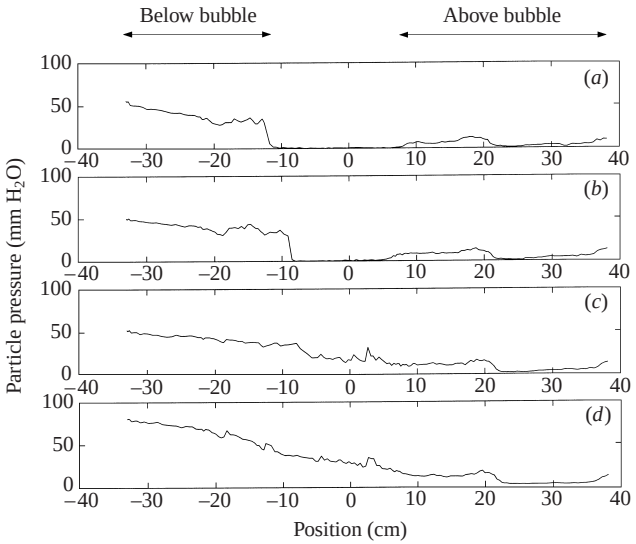


FIGURE 6. The particle pressure as a function of bed position in a bed of 0.5 mm glass beads. The four plots represent the 4 probes mounted 46 cm (18 in.) above the injection point. From top (*a*) to bottom (*d*), the probes are mounted 0, 5, 10, 15 cm from the bed centreline. The bed height is 109 cm (43 in.) and the effective bubble diameter just before eruption is 25.0 cm (9.8 in.).

these two outer probes are not crossed by the bubble; from time = 0 to 0.4 s the plots are almost the same as figures 4(*a*) and 4(*b*), but from time = 0.4 to 0.8 s the particle pressure rises and is nearly constant though still small in magnitude; from time = 0.8 s (at this point the bubble has just reached the two inner probes) until the bubble erupts from the bed at time = 1.8 s, the particle pressure rises until reaching its maximum value at bubble eruption. This shows that significant particle pressures are generated, not just below the bubble (1.2 < time < 1.8 s), but also to the sides of the bubble (0.8 < time < 1.2 s). Also, the particle pressure appears to be continuous within the particle phase (figures 4*c* and 4*d*) and only discontinuous at the bubble boundary (i.e. the abrupt jump in particle pressure as seen in figures 4(*a*) and 4(*b*) that occurs when the bubble wake is encountered by the two inner probes). And, the last noticeable feature is that, after bubble eruption, the particle pressure returns to its small minimum fluidization value for all four probe positions. Figure 6 shows the same particle pressure data as in figure 4 plotted as a function of the bubble's position within the bed.

Several mechanisms have been suggested for the generation of particle pressure in a fluidized bed. Commonly the particle pressure is attributed to the random, thermal-like, motion of particles (e.g. Batchelor 1988; Koch & Sangani 1999) such as those measured by Kumar *et al.* (1990) and Zenit *et al.* (1997) in liquid-fluidized beds. (Remember that liquid-fluidized beds are bubble free and expand nearly homogeneously and are thus not relevant to the phenomenon observed here.) Without much supporting evidence, Campbell & Wang (1991) speculated that a similar mechanism might be responsible for the small particle pressure they observed in a three-dimensional gas-fluidized bed held at minimum fluidization. But they found that relatively large particle pressures were generated in freely bubbling beds whose magnitudes scaled with the bubble size. Campbell & Wang (1991) argued that the particle pressure was generated by the large-scale movement of particles that were, *en masse*, disturbed by

the passage of a bubble much like the flow pattern of a fluid about a rising gas bubble; they suggested that as the bubble rises, it pushes particles out of the way and these particles can transmit a force out to the walls that is sensed as particle pressure.

However the current results indicate that this is not the case. Particle motion in a freely bubbling bed may appear to be chaotic and disorderly but Rowe & Partridge (1962) have observed that a single bubble in a two-dimensional bed causes a unique displacement of particles, and the streamlines around a bubble and its wake are similar to those in a potential flow field around a solid cylinder. If the particle pressures were generated by particle motion, then they would diminish far from the probe as the particle motion disappears while large pressures are generated far below a bubble where there is no gross motion of the bed. Also, since the particle motions are roughly symmetrical above and below the bubble, one would expect that the particle pressure they generate would also be roughly symmetrical, while the data show that the particle pressures below the bubble are of much greater magnitude than those above. It is also unlikely that these large particle pressures are a byproduct of bubble eruption since they are observed long before the bubble erupts.

Another possibility is that the particle pressures are caused by defluidization of sections of the bed. This can be expected as the presence of gas bubbles in the particle phase will alter the gas flow through the particle phase and may change how the weight of the bed is distributed between the particle and fluid phases. Since these experiments are conducted at minimum fluidization conditions, the particles in the bed are just barely fluidized before a bubble is injected (i.e. the upward gas flow is just sufficient to support the wieght of particles). After bubble injection, not only does a bubble steal part of the fluidizing gas, but it also disturbs the previously vertical alignment of the gas streamlines. (This will be shown in detail in the next section.) This affects the quality of particle fluidization and there will be portions of the bed for which the particles are no longer completely supported by the gas flow and become partially defluidized. The defluidized particles can only be supported across interparticle contacts so that their weight appears as a particle pressure.

The term 'defluidized' will be used often in this paper and it is worthwhile to define it clearly. It should not be confused with an ability or inability for the solid material to exhibit fluid-like behaviour. For example a dry granular material can often flow in a fluid-like fashion, but it not considered fluidized. The principle feature that makes a fluidized bed fluidized, is that the weight of the particle bed is supported by an upward motion of fluid. In that context, to be 'defluidized' means that the weight of the particles is not being supported by the fluid, in just the manner described in the last paragraph.

### 4.1. *'Slow' bubbles*

As for a bubble in a liquid, the rise velocity of a bubble in a fluidized bed is determined by the bubble size and is independent of the material that makes up the bed. However, the gas velocity required to achieve fluidization is determined by the bed material in the sense that small light materials require less fluidizing velocity that large heavy materials. Thus for large heavy materials, it is likely that the gas velocity through the bed is larger than the bubble rise velocity. Such bubbles are called 'slow bubbles'. Conversely, if the particles are small and light, the bubbles rise faster than the gas and are known as 'fast bubbles'. Now, the gas flow pattern around a bubble in a gas-fluidized bed is very different for the two cases. For a slow bubble, the gas must on the average pass through the bubble, entering at the base and exiting at the top. A fast bubble carries a portion of its own gas with it that recirculates through a

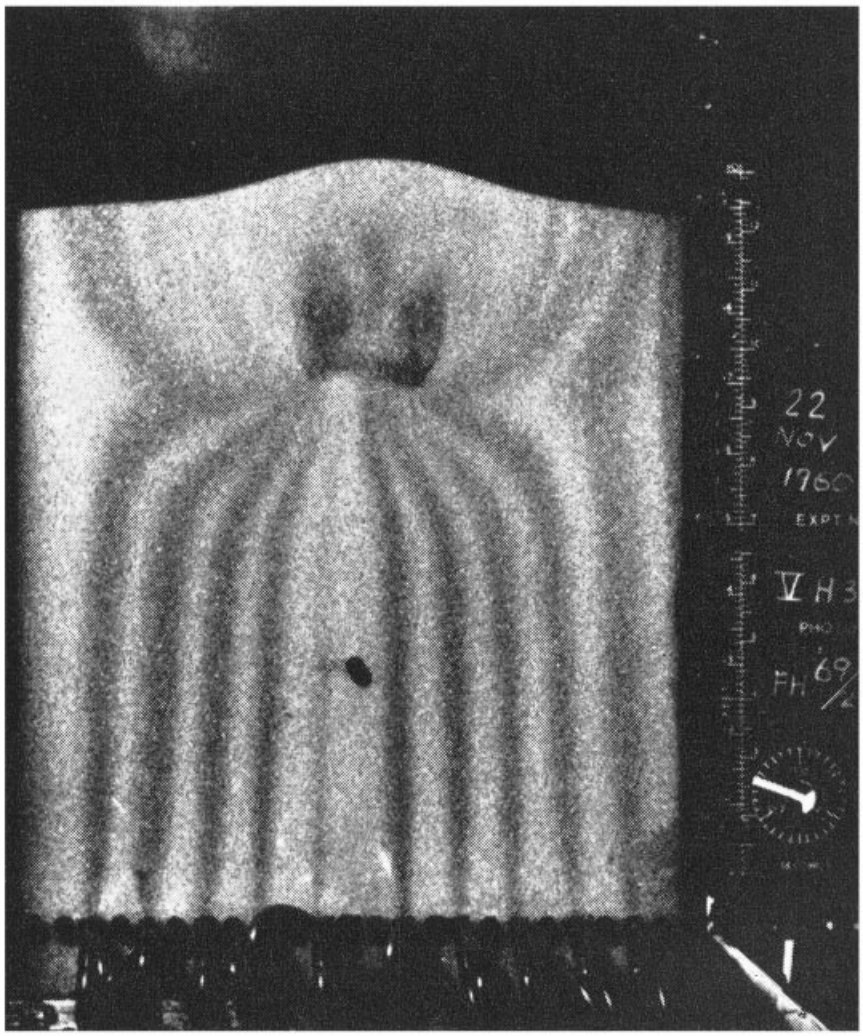


FIGURE 7. The gas flow around a slow bubble injected in a two-dimensional bed. Streaklines about the bubble are made visible by $NO_2$ injection. Note that the bubble attracts nearly all the gas in the bed. Reprinted from *Fluidisation*, First edition, P. N. Rowe, 'Experimental Properties of Bubbles,' p. 141, 1971, by permission of the publisher, Academic Press.

'cloud' about the bubble. As the above discussion indicates that the particle pressure arises from defluidization of the surrounding material, it is worthwhile to consider these two cases separately; we start with slow bubbles, as the 0.5 mm glassbead case shown in figure 4 is an example of a slow bubble.

Rowe (1971) documents a photograph (reproduced in figure 7) of the gas flow around a slow bubble rising in a two-dimensional gas-fluidized bed, made visible by $NO_2$ injection. There it can be seen that the passage of a bubble attracts almost all the gas within the bed. This can be anticipated as the bubble represents a void through which the gas may travel with nearly zero pressure drop; in contrast, the pressure drop the gas would experience while passing through the bed would approximately equal the hydrostatic weight of the bed. Consequently, the bubble represents a very attractive path and absorbs much gas from the particulate phase. This leaves surrounding areas

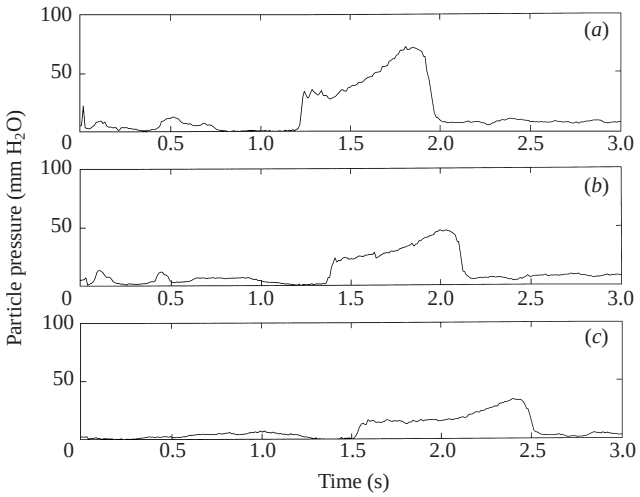


FIGURE 8. The effect of bubble diameter on the time history of the particle pressures in a bed of 0.5 mm glass beads. All the data are taken from the central pressure transducer. The bubble diameters at eruption are (*a*) 25.0 cm (9.8 in.), (*b*) 18.8 cm (7.4 in.) and (*c*) 13.7 cm (5.4 in.). The top trace is the same as shown in figure 4. In all cases the probes are mounted 46 cm (18 in.) above the injection point. Note that the magnitude of the particle pressures increases with the bubble size.

in the bed which are at best partially fluidized. Rowe's slow bubble photograph shows that the bubble attracts gas within a region extending to about two bubble diameters from its edge, nearly the width of the bed; this would indicate that the material on the sides of the bubble is at least partially defluidized. The photograph also shows that the direction of the gas flow deviates from the vertical in a region extending about one bubble diameter below the bubble, indicating another region of defluidized material. The majority of the gas must be leaving the top of the bubble, keeping that region fairly well fluidized, though this is not readily apparent from the photograph due to the mixing of tracer gases.

Figure 7 makes clear that the defluidization that results in the particle pressure arises from two sources: (i) the absorption of gas by the bubble and (ii) the deviated (non-vertical) gas streaklines caused by the attraction of the gas to the bubble. Once the material is defluidized, it is no longer supported by the gas flow and must simply rest on the material below it, generating the large particle pressures observed below the bubble (all four plots in figure 4). The steadily increasing particle pressure is related to the increasing weight of the defluidized material above the probes (note however that the maximum particle pressure is smaller than the hydrostatic value, indicating that the material is still partially fluidized). Obviously, this increasing weight is due to the fact that as the bubble moves further away from the probes, there is progressively more defluidized material above the probes. This may not be surprising as close to eruption the bubble's size rapidly increases (see figure 5) and it is to be anticipated that a larger bubble will absorb more gas, cause more defluidization and hence generate larger particle pressures. This is in concert with the observations by Campbell & Wang (1991) which show that the particle pressures scale with the bubble size.

Figure 8 shows the effect of bubble size on the pressure traces. These are all taken from the centreline pressure transducers; the largest diameter bubble is shown in plot (*a*), and the diameter decreases as one moves downwards. The most obvious feature

of these figures is that, as speculated above, the larger the bubble, the larger the generated particle pressures.

Also, Rowe's (1971) photograph, figure 7, indicates that the slow bubble deviates the gas flow over a region extending about one bubble diameter below the bubble. The results presented in figure 5 (figure 8*a*) were for a bubble with an effective diameter of 25.0 cm just before eruption. Thus, at eruption the maximum height of material above the probes was about one diameter and spans the defluidized zone as shown in the photograph. For the other two cases in figures 8(*b*) and 8(*c*), the effective bubble diameters just before eruption are 18.8 cm and 13.7 cm respectively and the height of the material above the probes at eruption is about 1.6 and 2.3 bubble diameters. Thus, according to the slow bubble picture figure 7, the probes are mounted below the span of the defluidized zone (i.e. in the zone where the gas-flow pattern has returned to normal). But the measurements still show a steadily increasing particle pressure below the bubble. It appears, as the bed is at minimum fluidization conditions, that the gas velocity generates just enough pressure drop to support the bed locally, but not enough to support the additional defluidized material being piled on from above. In other words, there is a zone of defluidized material that follows the bubble as it rises, the size of which is related to the size of the bubble. All this accounts for (i) why the particle pressure increases until eruption, (ii) why the pressures are never as large as would be expected if all the material above the probe were defluidized and (iii) why the pressures return quickly to normal after eruption. This conclusion is supported by further experiments that measured the particle pressures either for deeper beds than those shown here or for pressure probes placed at different locations in the bed. (See Rahman 1997 for details.) In no case did it appear that the particle pressure decreased as the bubble rose far beyond the probes.

Note that, in one sense, the bubble can be said to defluidize the entire bed. At minimum fluidization, the pressure drop through any section of the bed exactly balances the weight of the material therein. However, when the bubble defluidizes the material in its immediate environs, the weight of that material must be supported by the material below it. As the pressure drop is only sufficient to support the material locally, even in the parts of figure 7 where the gas streaklines are vertical, and not the additional weight of the defluidized material around the bubble, the gas no longer supports the entire weight of the solid material and in that sense is not fluidized as a whole. Furthermore, in this sense, the material below the bubble only becomes refluidized after bubble eruption. It is also interesting to note that the magnitude of the particle pressure generated appeared to change only with the bubble size and to be independent of either the position of the probes or the depth of the bed.

The three data sets shown in figure 8 represent bubbles that span 55%, 41% and 37% of the bed width just before eruption. Although not shown here, the defluidized region was observed to span the width of the bed in all cases, and despite the fact that the magnitude of the pressures increases with bubble diameter, the results were qualitatively similar in the regions off to the sides of the bubbles (see Rahman 1997 for the complete data for the smaller bubbles). Even the smallest bubble in figure 8(*c*) generates particle pressures that span the width of the bed. Looking carefully at Rowe's picture in figure 7, this should not be surprising since the bubble shown there is attracting gas from the bed almost all the way to the sidewalls. Consequently, a much larger two-dimensional bed with dimensions 234 cm in height, 117 cm in width and 1.28 cm deep was built to measure the particle pressure far to the side of the bubble; unfortunately, it was difficult to uniformly fluidize a bed with such large dimensions and a bubble, once injected, left large areas of the bed in a defluidized

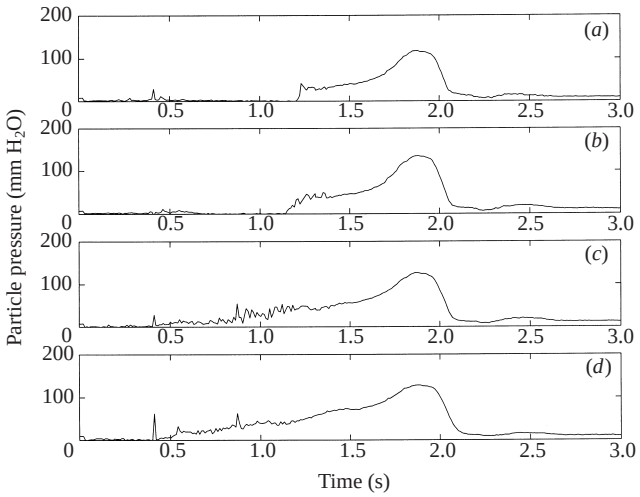


FIGURE 9. The time history of the particle pressures in a bed of 1 mm glass beads. The four plots represent four probes mounted 46 cm (18 in.) above the injection point 0, 5, 10, 15 cm from the bed centreline, (*a*)–(*d*) respectively. The bed height is 109 cm (43 in.) and the effective bubble diameter just before eruption is 24.5 cm (9.6 in.).

state that appeared to persist indefinitely. (This was evident because the particle pressures did not return to zero after the bubble had passed.) Apparently in such a large bed, there is enough room for favourable gas channels to form so that gas can avoid large sections of the bed. As a result, the data obtained from the large bed were inconsistent and non-repeatable. The original reason for building the larger bed was to have a bed wider than the region defluidized by a bubble (just how wide that would be is unknown). However, even with the larger bed, significant particle pressures were observed all the way out to the bed sidewalls, even for bubbles of the same sizes as shown above. Thus it was felt that there was little additional information to be gained from continuing work on such a large bed.

Note that a similar defluidization mechanism might explain the small particle pressures observed around minimum fluidization. Remember that minimum fluidization is defined as the minimum gas velocity by which the gross weight of the bed is supported by the gross pressure drop across it. However, it is unlikely that the actual gas flow through the apparently quiescent bed is actually uniform. It is much more likely that the gas finds weak paths or channels which it preferably follows through the bed. This would leave areas that are locally defluidized within the bed. This explanation is more satisfying than the thermalized particle speculation given by Campbell & Wang (1991) as no such motions are apparent within the bed.

The test material for all the data presented so far has been 0.5 mm glass beads. The obvious next step is to measure the particle pressure using larger glass beads (and thus ensuring that the bubbles remain 'slow' bubbles.) Figure 9 shows the time history of the particle pressures for a bed composed of 1 mm glass beads; the probes are mounted 46 cm (18 in.) above the injector and the bed depth is 109 cm (43 in.). The effective bubble diameter at eruption for this case is 24.5 cm (9.6 in.). As such these data are best compared with the 0.5 mm glass-bead data in figure 4. The particle pressure profiles in figure 9 show the same characteristic features as the 0.5 mm glass-bead results. That is, the particle pressure around a bubble is small above it, and significant particle pressures are generated to the sides and below the bubble;

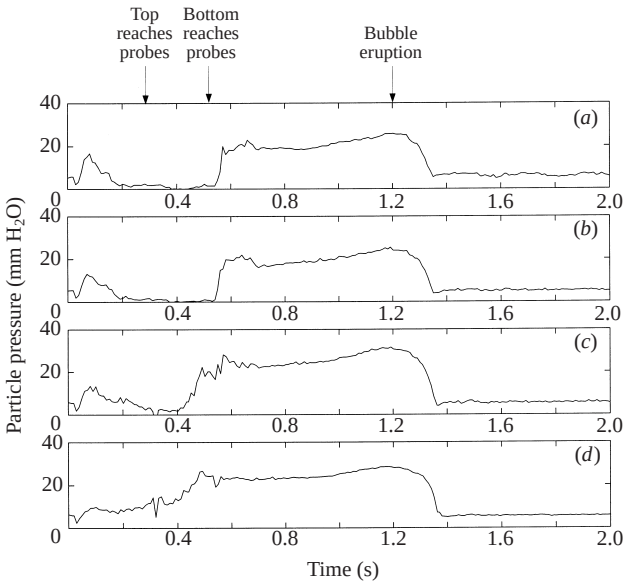


FIGURE 10. The time history of the particle pressures in a bed of 0.83 mm polystyrene beads. The four plots represent four probes mounted 15.2 cm (6 in.) above the injection point 0, 5, 10, 15 cm from the bed centreline, (*a*)–(*d*) respectively. The bed height is 83.8 cm (33 in.) and the effective bubble diameter just before eruption is 25.7 cm (10.1 in.).

also, the particle pressure downstream of the bubble steadily increases until bubble eruption (time = 1.8 s). All this shows that the particle pressure around 'slow' bubbles is not significantly affected by the particle size.

Finally, as Campbell & Wang (1991) showed that the particle pressure in a freely bubbling bed was proportional to the particle density, it makes sense to study a material with a different density than glass beads, but to be comparable with the previous data, a material that will still generate slow bubbles. Figure 10 shows the time history of the particle pressure for a bed composed of 0.83 mm polystyrene beads (density 1050 kg m$^{-3}$ compared to a density of 2500 kg m$^{-3}$ for the glass beads); the probes are mounted 15.2 cm (6 in.) above the injector and the bed depth is 83.8 cm (33 in.). The effective bubble diameter at eruption for this case is 25.7 cm (10.1 in.). Basically, the results show all of the same characteristics as the glass-bead studies presented above. (Note that the initial peak in particle pressure observed in figure 10, at about time = 0.1 s is a consequence of bubble injection.) The noticeable difference in these results is that the magnitude of the particle pressure below the bubble is considerably smaller than for glass beads for almost the same bubble size (e.g. compare figure 10 with figure 4 which has a comparable bubble diameter at eruption). This is not surprising since a given volume of defluidized glass beads will weigh more than the same volume of defluidized polystyrene beads (of course, assuming that the beads are packed in similar manners); hence, given that the density of glass is greater than that of polystyrene, the defluidization effect of glass beads should generate higher particle pressures than those generated by polystyrene beads.

### 4.2. *'Fast' bubbles*

As mentioned above, for small and/or light particles it is likely that the bed experiences fast bubbles, bubbles that rise faster than the interstitial gas. In this case, a portion

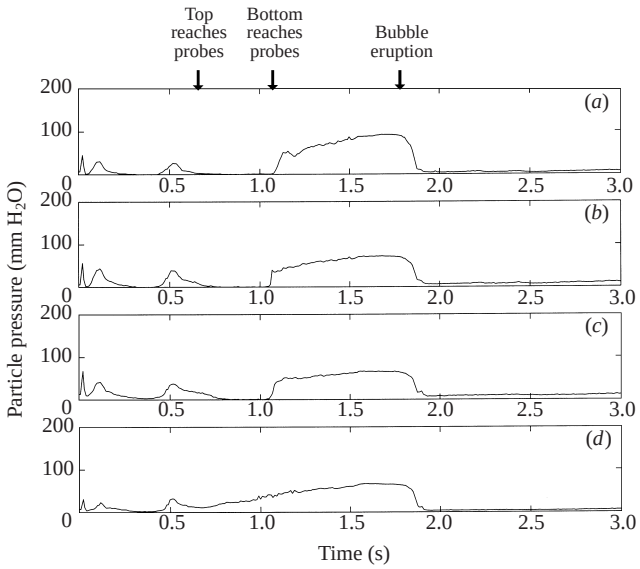


FIGURE 11. The time histories of the particle pressures in a bed of 0.25 mm glass beads (fast bubble). The four plots represent the 4 probes mounted 46 cm (18 in.) above the injection point 0, 5, 10, 15 cm from the bed centreline, (*a*)–(*d*) respectively. The bed height is 109 cm (43 in.) and the effective bubble diameter just before eruption is 26.1 cm (10.3 in.).

of the gas that travels through the bubble centre recirculates through a 'cloud' that surrounds the bubble and in that sense, the bubble carries some of its fluidizing gas along with it as it rises. Consequently, one might anticipate a different degree of defluidization. Unfortunately, it is not possible to visualize the gas flow pattern by tracer gases as in figure 7, as an injected tracer gas will never catch up with the bubble (although it is possible to visualize the cloud region, Rowe 1971). Consequently, it is difficult to anticipate the degree of gas-flow deviation caused by a 'fast' bubble.

Figure 11 shows the time history of the particle pressure for a fast bubble in a bed of 0.25 mm glass beads with a bed height of 109 cm (43 in.) with the probes mounted 45.7 cm (18 in.) above the injector. Here, the effective bubble diameter just before eruption is 26.1 cm (10.3 in.) and is thus best compared with figure 4. The plots are also marked with the times when the bubble crosses the probes and when the bubble erupts. Generally, the features are identical to the slow bubble case, i.e. below the bubble the particle pressure rises steadily and reaches a maximum value at bubble eruption. Despite the above speculation, this might well be expected since the degree of defluidization must reflect the amount of gas that must be 'stolen' from the surrounding bed to form the bubble. From that point of view, the degree of defluidization should be a function of bubble size, just as suggested by the results of Campbell & Wang (1991). The only major difference between fast and slow bubble behaviour is above the bubble where a significant particle pressure peak is observed (at about time = 0.5 s in figure 11). (Note that bubble injection probably accounts for the initial two particle pressure peaks that appear early in the trace, up to about time = 0.2 s.)

The relatively large initial peak at a time about 0.5 s may be a result of defluidization resulting from the encounter between the probes and the cloud that surrounds the bubble. As the cloud represents a layer of gas recirculating around the bubble, the gas flows downwards around the sides of the bubble. As an upward gas flow is

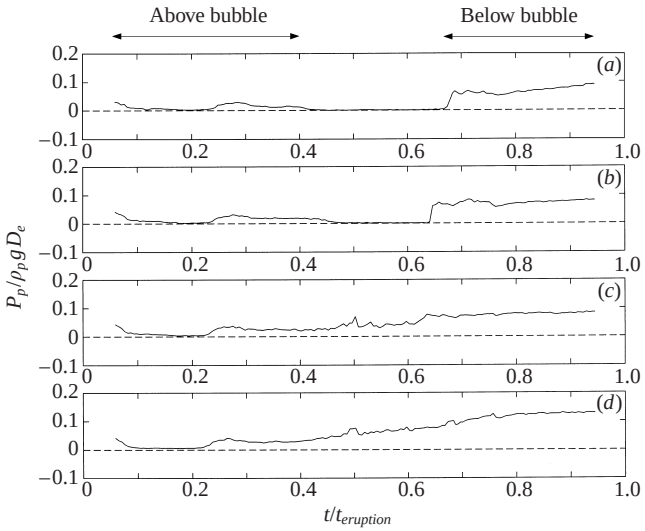


FIGURE 12. Time traces of the scaled particle pressure in a bed of 0.5 mm glass beads (slow bubble). The four plots come from four probes mounted 46 cm (18 in.) above the injection point, and 0, 5, 10, 15 cm from the bed centreline (*a*)–(*d*) respectively. The bed height is 109 cm (43 in.) and the effective bubble diameter just before eruption is 25.0 cm (9.8 in.). (The unscaled particle pressure data are in figure 4.)

responsible for keeping the material fluidized, this downward flow may well enhance the local defluidization. Note that the size of this peak is slightly larger towards the sides of the bubble where the downward gas velocity is the largest and where one would thus expect the largest defluidization.

### 4.3. *Particle pressure scaling*

All this suggests that the two important parameters responsible for the generation of particle pressure are the bubble size and the density of the solid material. This is not surprising in view of the results of Campbell & Wang (1991). Their results for a freely bubbling three-dimensional bed showed that the average particle pressure was proportional to the product of the particle density and the equivalent bubble diameter, that is, $P_p/\rho_p g D_e$ is approximately a constant (here $P_p$ is the particle pressure, $\rho_p$ is the density of the solid material, $g$ is the gravitational acceleration and $D_e$ is the effective bubble diameter). Figure 12 shows the instantaneous particle pressure data from figure 4 scaled according to the above rule using the instantaneous value of the effective bubble diameter. (Note that these figures terminate at bubble eruption as the bubble diameter is undefined beyond that point.) The details are the same as in figure 4. The time axis is scaled with the eruption time. The most important feature of these plots is that below the bubble the value of $P_p/\rho_p g D_e$ is nearly constant and does not vary across the span of the bed. Thus, the increasing particle pressure below the bubble as seen in figure 4 is a direct consequence of the increasing bubble size as the bubble travels upwards through the bed. This is not surprising since a larger bubble is a larger void which presents more surface area and attracts more gas from the bed, causing more material to be defluidized, which results in an increased particle pressure. Figures 13 and 14 show the instantaneous scaled particle pressure ($P_p/\rho_p g D_e$) on the centreline probe for a number of particle sizes, materials, bed heights, probe positions and bubble sizes. In the captions of

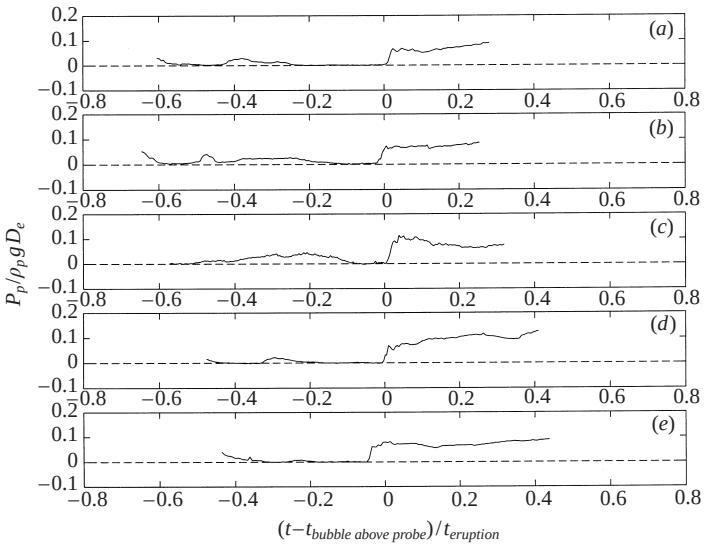


FIGURE 13. Time traces of the centreline scaled particle pressure for 0.5 mm glass beads (slow bubble): (*a*) $H_b$ = 109 cm (43 in.), $H_p$ = 46 cm (18 in.), $D_b$ = 25.0 cm (9.8 in.); (*b*) $H_b$ = 109 cm (43 in.), $H_p$ = 46 cm (18 in.), $D_b$ = 18.8 cm (7.4 in.); (*c*) $H_b$ = 109 cm (43 in.), $H_p$ = 46 cm (18 in.), $D_b$ = 13.7 cm (5.4 in.); (*d*) $H_b$ = 127 cm (50 in.), $H_p$ = 46 cm (18 in.), $D_b$ = 24.6 cm (9.7 in.); (*e*) $H_b$ = 109 cm (43 in.), $H_p$ = 30.5 cm (12 in.), $D_b$ = 25.7 cm (10.1 in.).

figures 13 and 14 the bed height is labelled as $H_b$, the distance of the probe above the injection point is labelled as $H_p$, and the effective bubble diameter just before eruption is labelled as $D_b$. The time axis is non-dimensionalized by subtracting the approximate time at which the bubble is just above the probe (or crosses the probe position in the bed) and scaling the result with the eruption time. This allows several scaled particle pressure data sets to be conveniently and comparatively visualized on a single figure.

The most obvious feature of all of these figures is that the value of $P_p/\rho_p g D_e$ below the bubble is uniformly equal to about 0.1. This value takes into account the effect of bubble size as shown in figure 13(*a–c*). It is independent of the height of material above the probe (varied by changing the depth of the bed and/or the probe position as shown in figures 13(*d, e*) and 14(*a*). Figure 14(*b*), the data for 1 mm glass beads, show that the scaled pressure is also independent of particle size and figure 14(*c*) for 0.83 mm polystyrene beads indicates that it accurately handles the effect of a change in the density of the bed material. Finally, figure 14(*d, e*) shows the centreline scaled particle pressures ($P_p/\rho_p g D_e$) for two different sized 'fast' bubbles in a bed of 0.25 mm glass beads, once again resulting in the same value.

Though figures 13 and 14 depict the centreline scaled pressure, it should be noted that below the bubble the scaled particle pressure ($P_p/\rho_p g D_e$) is roughly constant in magnitude and has a value close to 0.1 across the span of the bed, i.e. at positions offset from the bed centreline. This was illustrated above in figure 12, and for brevity is not repeated herein for all the other cases of figures 13 and 14.

### 4.4. *Multiple bubbles*

Figure 15(*a*) shows the particles pressure in a freely bubbling bed of 0.5 mm glass beads generated by a gas velocity 5% above minimum fluidization. Figure 15(*b*) shows a detail of a single bubble that very nearly crosses the centre probe. One can see that

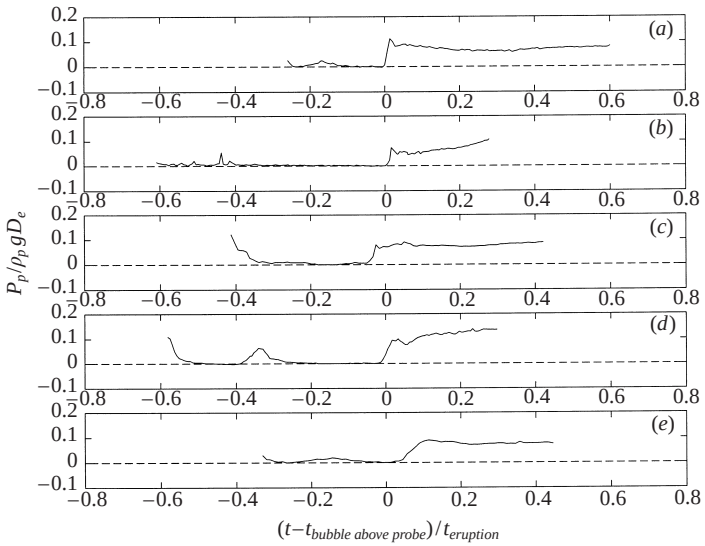


FIGURE 14. Time traces of the centreline scaled particle pressure: (*a*) 0.5 mm glass beads (slow bubble), $H_b = 83.8$ cm (33 in.), $H_p = 15.2$ cm (6 in.), $D_b = 13.9$ cm (5.5 in.); (*b*) 1 mm glass beads (slow bubble), $H_b = 109$ cm (43 in.), $H_p = 46$ cm (18 in.), $D_b = 24.5$ cm (9.6 in.); (*c*) 0.83 mm polystyrene beads (slow bubble), $H_b = 83.8$ cm (33 in.), $H_p = 15.2$ cm (6 in.), $D_b = 25.7$ cm (10.1 in.); (*d*) 0.25 mm glass beads (fast bubble), $H_b = 109$ cm (43 in.), $H_p = 46$ cm (18 in.), $D_b = 26.1$ cm (10.3 in.); (*e*) 0.25 mm glass beads (fast bubble), $H_b = 68.6$ cm (27 in.), $H_p = 15.2$ cm (6 in.), $D_b = 11.2$ cm (4.4 in.).

the character of these bubbles is very different from the single bubbles observed so far. In particular, the maximum particle pressure is observed soon after the probes encounter the bubble wake, and decreases thereafter until the bubble erupts. This is in stark contrast to the single bubble behaviour for which the maximum particle pressure occurs at eruption. Also note that though the bubble size at eruption for this trace is approximately the same as that of the single bubble traces in figure 4, the magnitude of the maximum particle pressure is about half. The traces shown in figure 15 are similar to those observed in a three-dimensional bed by Campbell & Rahman (1992) held 60% above minimum fluidization. It is also nearly identical to the schematic in Rathbone *et al.* (1989) who measured transient normal and shear stresses on the surface of a tube in a freely bubbling two-dimensional gas-fluidized bed using a piezo-electric force transducer. The gas flow pattern around a 'slow' bubble, figure 7, suggests that gas being absorbed by the bubble should exit from the bubble roof, hence at least partially refluidizing any defluidized material being piled on by a leading bubble. Thus, it is very likely that the refluidization from other bubbles in a freely bubbling bed is the cause of the change in behaviour of the particle pressure as seen in figure 15.

Figure 16 is the time history of the particle pressure for two bubbles, the second bubble being injected 1 s after the first. The figure is also marked with the times when the bubbles cross the probes and the points at which the bubbles erupt from the bed. The particle pressures generated below the leading bubble are significantly different from the typical particle pressure profiles generated by single bubbles. The leading bubble defluidizes material in the usual manner until the trailing bubble is injected at time = 1.0 s. At this point the leading bubble is covering the two centre probes. But once the leading bubble crosses the probes a somewhat flat particle pressure

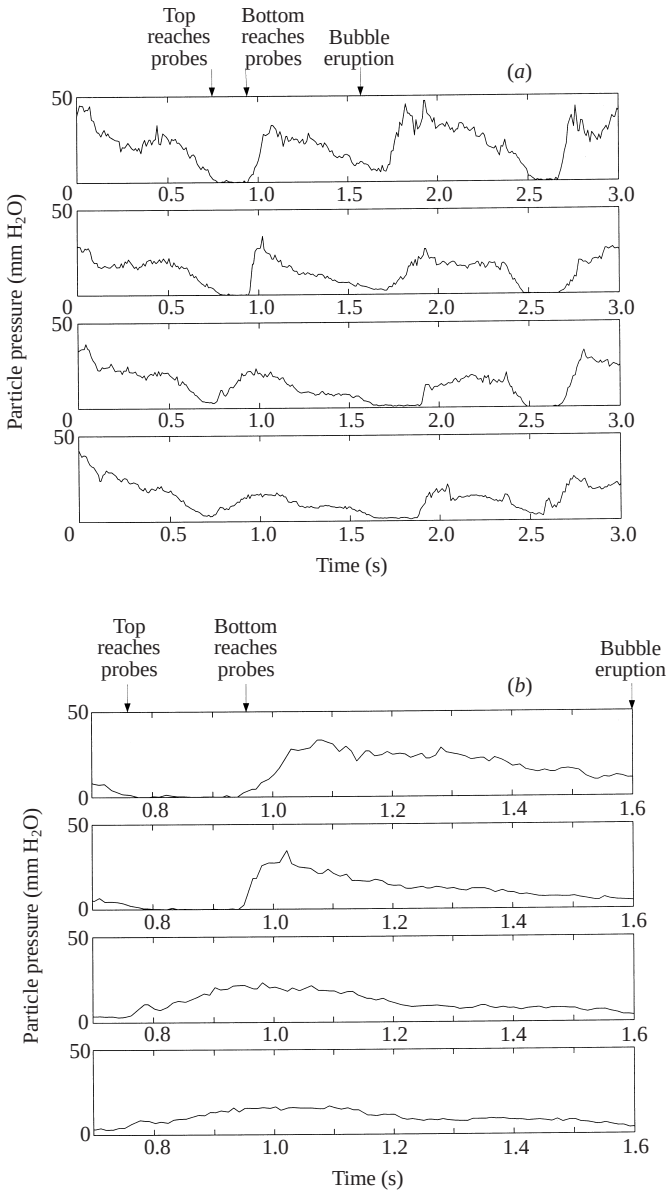


FIGURE 15. Particle pressures generated in a freely bubbling bed of 0.5 mm glass beads. The probes are mounted 46 cm (18 in.) above the injector, the bed height is 109 cm (43 in.), and the fluidization velocity is 60% above minimum fluidization. (*a*) A time trace showing several bubble passages. (*b*) A detail of the trace from a bubble that passes nearly up the centre of the channel.

profile is generated until the leading bubble erupts, at which point there is a marked reduction in the particle pressure value. It appears that the high gas velocity exiting the top of the trailing bubble is partially refluidizing the defluidized material about the leading bubble. On the other hand, after the leading bubble erupts (time = 1.4 s) the behaviour of the particle pressures generated by the trailing bubble is exactly the same as that of single bubbles. Thus, this two-bubble injection situation helps explain

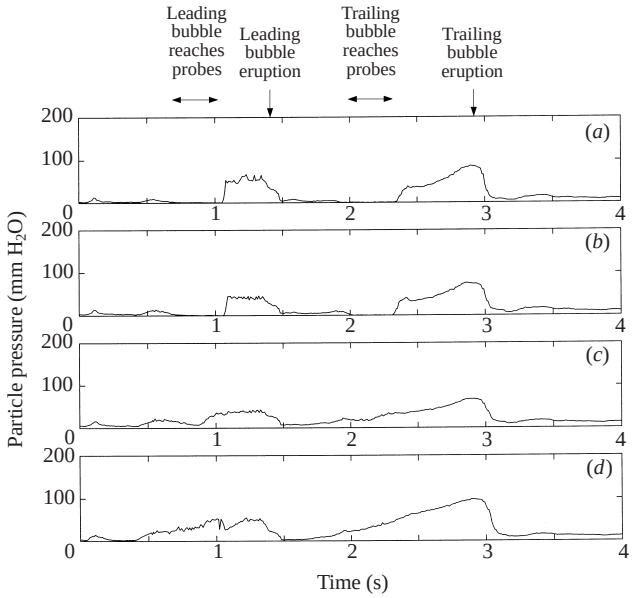


FIGURE 16. Particle pressures generated by two-bubble injection (the second bubble being injected 1.0 s after the first in a bed of 0.5 mm glass beads, held at minimum fluidization. The probes are mounted 46 cm (18 in.) above the injection point 0, 5, 10, 15 cm from the bed centreline, (*a*)–(*d*) respectively. The bed height is 109 cm (43 in.). The effective bubble diameters just before eruption for the leading and trailing bubbles are 31.2 cm (12.3 in.) and 23.4 cm (9.2 in.) respectively.

that the difference in particle pressure generation between a single bubble and a freely bubbling bed is due to the presence of other bubbles.

Note that the results shown in figure 16 do not exactly match those in figure 15 even though they do show a significant impact of the trailing bubble on its predecessor. This is perhaps due to the relative positions of the bubbles. As the two bubbles in figure 16 are injected from the same injector, the trailing bubble exactly follows the leading one. But a close examination of figure 4(*a*) shows that the trailing bubble actually crosses the third and fourth probe (and the top of the bubble clearly encounters the fourth probe first, indicating that the centre is closer to the fourth probe than the third). Thus the centre of the trailing bubble is around 15 cm or two-thirds of a diameter off to the side of the leading bubble. The difference in the gas flow patterns in those two regions could explain the differences in the observed particle pressure profiles.

All this raises the issue of the marked difference between single-bubble experiments and measurements performed in a freely bubbling bed. Artificially injected single-bubble experiments are very popular in the fluidization community and they may yield a wealth of information about single bubbles. But care must be taken in comparing a single bubble in a fluidized bed and bubbles in a freely bubbling bed. As has been shown above the interaction of bubbles can result in significantly different behaviour.

But there is perhaps another explanation for the difference between the data in figure 15 and all the previous data from beds held at minimum fluidization. Above minimum fluidization, there is more gas available to support the weight of the bed. Much of that extra gas is lost in bubbles, but it is possible that much gas remains within the emulsion phase, allowing the material far from the bubble to support the defluidized region around the bubble and to become locally refluidized.

## 5. Conclusions

This paper describes measurements of the particle pressure exerted by the passage of an injected bubble on the vertical face of a two-dimensional fluidized bed which is otherwise held at minimum fluidization. The particle pressure generated around single bubbles in a gas-fluidized bed is most significant only below and to the sides of the bubble; above the bubble the magnitude of the particle pressure is relatively small. The particle pressure below the bubble was observed to increase as the bubble moves away and reaches a maximum magnitude at bubble eruption, after which it quickly returns to its small value at minimum fluidization. Also, the effect of the bubble is felt all the way to the bed sidewalls, even if the bubble is small compared to the bed width. This scenario of the particle pressure behaviour in gas-fluidized beds holds true for bubbles of different sizes, particles of different sizes and densities, different bed heights and probe positions, as well as for both 'slow' and 'fast' bubbles. It should be noted however, that all the materials used in this study fall into a Geldart B classification and show no initial region of homogeneous fluidization as are observed for smaller and finer Geldart A particles.

On the basis of less complete observations, Campbell & Wang (1991) suggested that the particle pressures were generated by large-scale movement of particles caused by the passage of a bubble. But, the results presented herein show that particle motion is not a significant contributor to the particle pressure around a single bubble. These results indicate that the particle pressure generated around single bubbles in gas-fluidized beds is a result of the defluidization of material in the particle phase. The passage of a bubble in a homogeneously fluidized bed attracts gas away from the particle phase – this leads to regions in the bed where the local gas velocity is not sufficient to fluidize the solid particles, leaving them unsupported or defluidized. It is the weight of this defluidized material that is sensed as particle pressure.

These results also show that the magnitude of the particle pressure, downstream of the bubble, depends on the bubble size and the solid material density. If the particle pressure is scaled according to the rule suggested by Campbell & Wang (1991), $P_p/\rho_p g D_e$ where $P_p$ is the transient particle pressure, $\rho_p$ is the solid density, $g$ is the acceleration due to gravity, and $D_e$ is the effective bubble diameter, all the particle pressure data, below the bubble, collapse to an approximately constant value 0.1. That is,

$$\frac{P_p}{\rho_p g D_e} \approx \text{constant} \approx 0.1$$

holds true for 'slow' and 'fast' bubbles as well as different bubble sizes, solid material densities, solid particle sizes and depths of the bed. But, aside from the universality of this particle pressure scaling, it is also noteworthy that the steadily increasing particle pressure downstream of a bubble is a direct consequence of the steadily increasing bubble size. The value observed here is slightly larger than but comparable to the three-dimensional value 0.08 found by Campbell & Wang, even though that data represented a time-averaged particle pressure and not just the value in the particle wake. Still the fact that the Campbell & Wang (1991) results are of the same order as these suggests that there is little change on going from the two-dimensional bed studied here to a three-dimensional bed.

The particle pressure behaviour in a freely bubbling gas-fluidized bed is markedly different from that around a single bubble. In a freely bubbling bed the maximum particle pressure is observed directly after the probes encounter the bubble wake, and not at eruption as is observed for single bubble. This is similar to the results

of Campbell & Rahman (1992) and Rathbone *et al.* (1989). A similar, though not identical effect was achieved by injecting multiple bubbles into the bed. This indicated that the presence of multiple bubbles and their interactions diminish the effect of defluidization in the bed, most likely by refluidization by the gas exiting the roofs of trailing bubbles.

Note that the particle pressures measured here cannot be accounted for by kinetic theory models such as that presented in Koch & Sangani (1999). There are many indications that this is the case, such as that the pressures are large far below the bubble where there is no agitation to generate the necessary granular temperatures. But the most telling observation is that these particle pressures are independent of the particle diameter, which is the microscopic length scale appearing in all kinetic theory models. Furthermore, because these results are independent of the particle diameter, and of the fluidizing gas velocity they are therefore independent of the Stokes number for the particles. The most likely possibility is that the defluidized particles are supported elastically across networks of particles, which results in the measured particle pressures, but that supposition is based on the lack of any alternative explanation.

This work was supported by the US Department of Energy under grant Grant # DE-FG03-91ER14223 for which the authors are very grateful.

## REFERENCES

Agbim, J. A., Nienow, A. W. & Rowe, P. N. 1971 Interparticle forces that suppress bubbling in gas-fluidized beds. *Chem. Engng Sci.* **26**, 1293.

Anderson, T. B. & Jackson, R. 1968 Fluid mechanical description of fluidized beds: stability of the state of uniform fluidization. *Ind. Engng Chem. Fundam.* **7**, 12.

Batchelor, G. K. 1988 A new theory of the instability of a uniform fluidized bed. *J. Fluid Mech.* **193**, 75.

Campbell, C. S. & Rahman, K. 1992 An improved particle pressure transducer. *Meas. Sci. Technol.* **3**, 709.

Campbell, C. S. & Wang, D. G. 1990 A particle pressure transducer suitable for use in gas-fluidized beds. *Meas. Sci. Technol.* **1**, 1275.

Campbell, C. S. & Wang, D. G. 1991 Particle pressures in gas-fluidized beds. *J. Fluid Mech.* **227**, 495.

Foscolo, P. V. & Gibilaro, L. G. 1987 Fluid dynamic stability of fluidized suspensions: the particle bed model. *Chem. Engng Sci.* **39**, 1489.

Garg, S. K. & Pritchett, J. W. 1975 Dynamics of gas-fluidized beds. *J. Appl. Phys.* **46**, 4693.

Ham, J. M., Thomas, S., Guazzelli, E., Homsy, G. M. & Anselmet, M. C. 1990 An experimental study of the stability of liquid-fluidized beds. *Intl J. Multiphase Flow* **16**, 171.

Jackson, R. 1963 The mechanics of fluidized beds: Part I: the stability of the state of uniform fluidization. *Trans. Inst. Chem Engrs* **41**, 13.

Jackson, R. 1985 Hydrodynamic stability of fluid-particle systems. In *Fluidization* (ed. J. F. Davidson, R. Clift & D. Harrison), 2nd edn, pp. 47–72. Academic.

Koch D. L. & Sangani A. S. 1999 Particle pressure and marginal stability limits for a homogeneous monodisperse gas-fluidized bed: kinetic theory and numerical simulations. *J. Fluid Mech.* **400**, 229.

Kumar, S., Hart, D. P. & Brennen, C. E. 1990 Granular pressure measurements in fluidized beds. *ASME Cavitation and Multiphase Flow Forum, June 1990, Toronto, Canada.*

Murray, J. D. 1965 On the mathematics of fluidization. Part 1. Fundamental equations and wave propagation. *J. Fluid Mech.* **21**, 465.

Mutsers, S. M. P. & Rietema, K. 1977 The effect of interparticle forces on the expansion of a homogeneous gas-fluidized bed. *Powder Technol.* **18**, 239.

PIGFORD, R. L. & BARON, T. 1965 Hydrodynamic stability of a fluidized bed. *Ind. Engng Chem. Fundam.* **4**, 81.

RAHMAN, K. 1997 Particle pressures generated around bubbles in gas-fluidized beds. PhD Thesis, University of Southern California, Los Angeles, California.

RATHBONE, R. R., GHADIRI, M. & CLIFT, R. 1989 Measurement of particle velocities and associated stresses on immersed surfaces in fluidized beds. In *Fluidization VI* (ed. J. R. Grace, L. W. Shemilt & M. A. Bergougnou), p. 629. Engineering Foundation.

RIETEMA, K., COTTAAR, E. J. E. & PIEPERS, H. W. 1993 The effect of interparticle forces on the stability of gas-fluidized beds – II. theoretical derivation of bed elasticity on the basis of Van Der Waals forces between powder particles. *Chem. Engng Sci.* **48**, 1687.

RIETEMA, K. & PIEPERS, H. W. 1990 The effect of interparticle forces on the stability of gas-fluidized beds – I. experimental evidence. *Chem. Engng Sci.* **45**, 1627.

ROWE, P. N. 1971 Experimental properties of bubbles. In *Fluidization* (ed. J. F. Davidson & D. Harrison), pp. 121–191. Academic Press, London.

ROWE, P. N. & PARTRIDGE, B. A. 1962 Particle movement caused by bubbles in a fluidized beds. *Symposium on the Interaction between Fluids and Particles, London*, p. 135. Inst. Chem. Engrs.

TSINOTIDES, S. C. & JACKSON, R. 1993 The mechanics of gas-fluidized beds with an interval of stable fluidization. *J. Fluid Mech.* **255**, 237.

ZENIT, R., HUNT, M. L. & BRENNEN, C. E. 1997 Collisional particle pressure measurements in solid-liquid flows. *J. Fluid Mech.* **353**, 261.